ACS APPLIED MATERIALS & INTERFACES

Research Article

www.acsami.org

Boron/Nitrogen Co-Doped Helically Unzipped Multiwalled Carbon Nanotubes as Efficient Electrocatalyst for Oxygen Reduction

Alireza Zehtab Yazdi,[†,‡] Huilong Fei,[‡] Ruquan Ye,[‡] Gunuk Wang,[‡,⊥] James Tour,*[,‡,§] and Uttandaraman Sundararaj*[,†]

[†]Polymer Processing Group, Department of Chemical and Petroleum Engineering, University of Calgary, 2500 University Drive, NW, Calgary, Alberta T2N1N4, Canada

[‡]Department of Chemistry, [§]Smalley Institute for Nanoscale Science and Technology, Department of Materials Science and NanoEngineering, Rice University, 6100 Main Street, Houston, Texas 77005, United States

Supporting Information

ABSTRACT: Bamboo structured nitrogen doped multiwalled carbon nanotubes have been helically unzipped, and nitrogen doped graphene oxide nanoribbons (CN_x-GONRs) with a multifaceted microstructure have been obtained. CN_x-GONRs have then been codoped with nitrogen and boron by simultaneous thermal annealing in ammonia and boron oxide atmospheres, respectively. The effects of the codoping time and temperature on the concentration of the dopants and their functional groups have been extensively investigated. X-ray photoelectron spectroscopy results indicate that pyridinic and BC_3 are the main nitrogen and boron functional groups, respectively, in the codoped samples. The oxygen reduction reaction (ORR) properties of the samples have been measured in an alkaline electrolyte and compared with the state-of-the-art Pt/C (20%) electrocatalyst. The results show that the nitrogen/boron codoped graphene nanoribbons with helically unzipped structures (CN_x/CB_x-GNRs) can compete with the Pt/C (20%) electrocatalyst in all of the key ORR properties: onset potential, exchange current density, four electron pathway selectivity, kinetic current density, and stability. The development of such graphene nanoribbon-based electrocatalyst could be a harbinger of precious metal-free carbon-based nanomaterials for ORR applications.

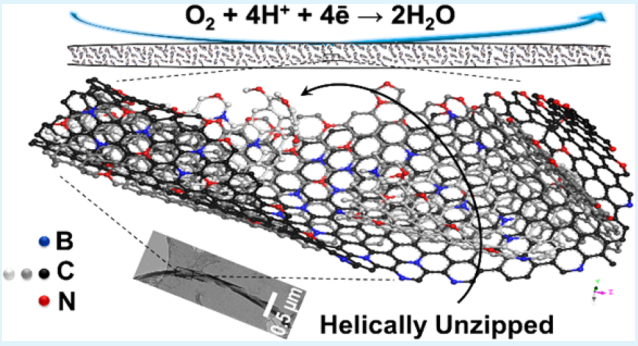

KEYWORDS: *bamboo structures, helical unzipping, graphene nanoribbons, codoping, oxygen reduction*

INTRODUCTION

The oxygen reduction reaction (ORR) that occurs at the cathode of the current state-of-the-art fuel cells and metal−air batteries has recently become an important design parameter.[1−3] Thus far, platinum (Pt)-based materials are widely considered to be the most practical electrocatalyst for ORR. However, the sluggish reduction process, limited stability, prohibitive cost, and the rarity of Pt have stimulated extensive research for the development of more efficient, durable, and inexpensive alternatives.[4−6] Carbon nanomaterials have been the main focus of research toward a replacement of precious-metal systems.[7,8]

Graphene-based, metal-free electrocatalysts are at the forefront of carbon nanomaterials research directed toward alternatives to Pt catalysts. Reduced graphene was originally reported as an efficient ORR catalyst that demonstrated fast electron transfer kinetics and excellent electrocatalytic activity.[9] Since then, numerous experimental efforts have been devoted to enhance the ORR performance of metal-free graphene by carrier injection or extraction, known as chemical doping.[10−22] In this case, some of the carbon atoms in the sp^2 network are substituted by heteroatoms of approximately the same radius, such as nitrogen,[10−16] boron,[17−19] sulfur,[20,21] or phosphorus.[22]

A review of the experimental and theoretical literature on electrocatalysts suggests that the presence of nitrogen functional groups in the graphene structure is needed for high electrocatalytic performance.[5,6,16] In particular, a recent synchrotron X-ray photoelectron spectroscopy (XPS) study before and after ORR testing showed that the carbon atoms in the nearby pyridinic nitrogen groups are much more active than pyrrolic and quaternary nitrogen.[16] It is also suggested that the pyridinic species on the edges are more likely to be involved in the catalytic process than basal plane pyridinics. In addition to single-atom type doping of graphene, there are a few experimental attempts that reported even higher ORR performance when other heteroatoms such as sulfur or boron supplement the nitrogen.[18,19,21] This type of synergistic structure may be synthesized via a simultaneous exposure of

Received: February 3, 2015
Accepted: March 20, 2015
Published: March 20, 2015

DOI: 10.1021/acsami.5b01067
ACS Appl. Mater. Interfaces 2015, 7, 7786−7794

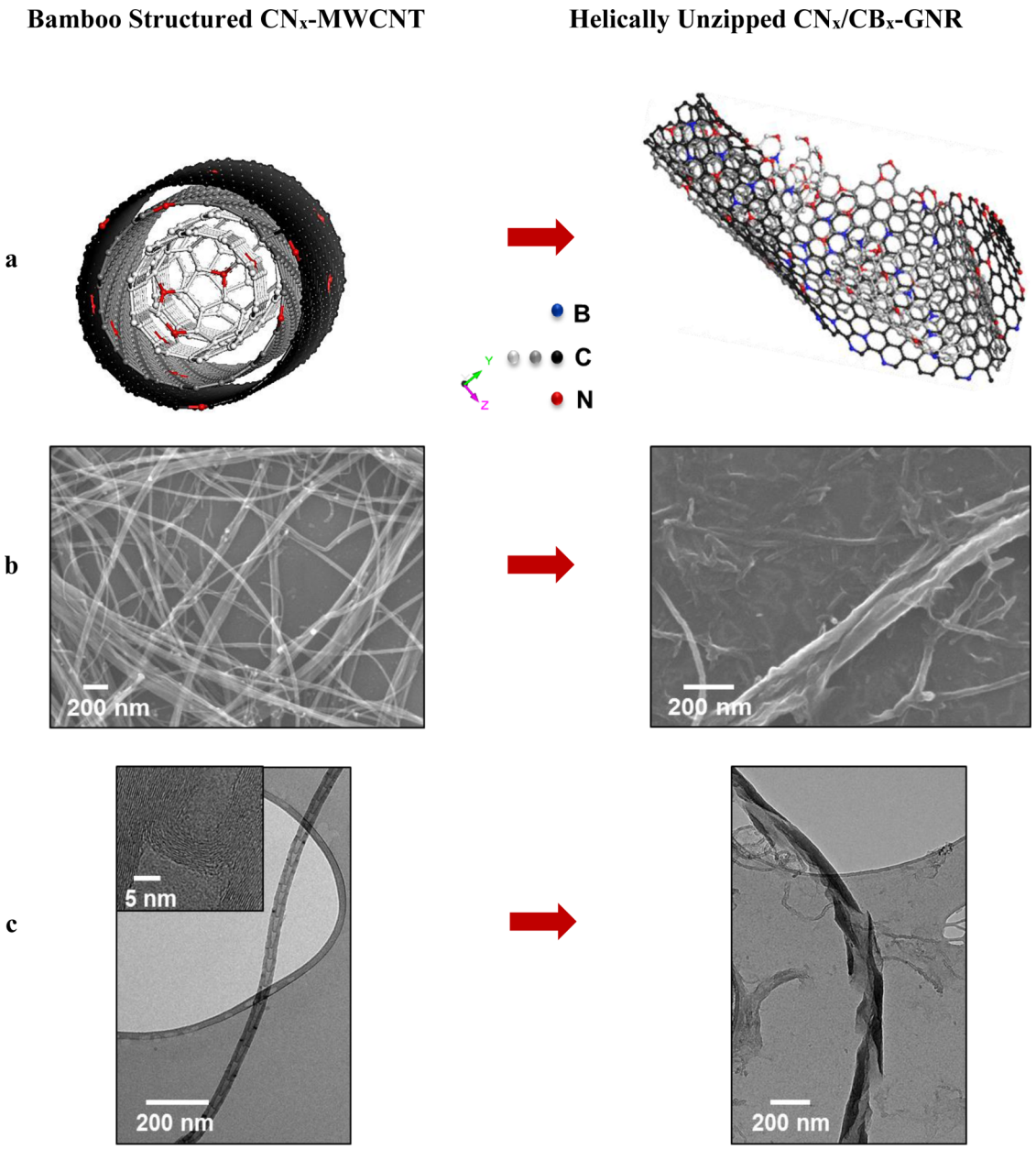

Figure 1. (a) Schematic illustration of a bamboo structured, nitrogen doped, multiwalled carbon nanotube (CN_x-MWCNT, left) and nitrogen/boron codoped graphene nanoribbon (CN_x/CB_x-GNR, right) depicting helically unzipped structure, (b) SEM image of several starting CN_x-MWCNTs (left) and a helically unzipped structure of CN_x/CB_x-GNR (right), and (c) HRTEM image of an individual CN_x-MWCNT with bamboo compartments (capped short carbon nanotubes, inset) that are sequentially located inside the main nanotube (left) and a helically unraveled microstructure of the resultant graphene nanoribbon (right).

graphene to both dopants' precursors,[18,21] named "co-doped graphene", or a two-step doping process,[19] named "tandem-doped graphene". Nevertheless, there remains an ongoing debate in the literature on whether metal-free graphene can indeed compete with Pt-based electrocatalysts in their key ORR properties, namely, onset potential, exchange current density, four electron pathway selectivity, kinetic current density and stability.[5]

Graphene nanoribbons (GNRs) are narrow elongated strips of graphene with ultrahigh aspect ratio and edge dependent properties that have recently attracted much interest as an excellent candidate to replace Pt catalysts, particularly if obtained by unzipping of multiwalled carbon nanotubes (MWCNTs). GNRs have a much higher edge-to-plane ratio than the sheet-like graphene. According to several density functional theory (DFT) calculations, the reactivity of edge-abundant structures in GNRs may significantly enhance ORR performance by decreasing the energy barriers of oxygen adsorption and first electron transfer.[5,16,18,19,21,23] Similar to graphene, it is also suggested that incorporation of nitrogen species into the nanoribbon's structure, particularly pyridinic species, would further enhance the reactivity of the edges. DFT calculations showed that the neighbor carbon atoms of pyridinic nitrogen have favored atomic charges that can induce the ORR process through the absorption of the intermediate products, the formation of C—O bonds, and the disassociation of O—O bonds.[5,16,19,21] Increasing the rate of the first electron transfer and the preference for the four electron reduction

DOI: 10.1021/acsami.5b01067
ACS Appl. Mater. Interfaces 2015, 7, 7786−7794

pathway (rather than the two electron) are the main mechanisms that improve two of the key ORR properties.[5,23]

Despite the unique electrocatalytic properties of edges, few experiments have been conducted which exploit GNRs for ORR applications.[24−27] In an early attempt, Li et al.[24] reported an excellent ORR performance of a nitrogen doped, partially unzipped, carbon nanotube/graphene mixture. Then, silver/GNR composite[25] and nitrogen doped GNRs[26,27] have been proposed as electrocatalysts for oxygen reduction. These GNR-based catalysts, however, can only compete with Pt in a few of the key ORR properties. For instance, none of them have an onset potential as low as the current state-of-the-art Pt catalysts. Therefore, developing GNR electrocatalysts with abundant active sites (edges) that can compete with Pt in all ORR properties is advantageous to replacement of precious metals by inexpensive carbon-based nanomaterials.

Our group recently reported helical unzipping mechanisms of the bamboo structured, nitrogen doped, multiwalled carbon nanotubes (CN_x-MWCNTs) via a chemical treatment to obtain nitrogen doped graphene oxide nanoribbons (CN_x-GONRs).[28−30] In this study, these CN_x-GONRs with multifaceted structures are simultaneously exposed to ammonia (NH_3) gas and boron oxide (B_2O_3) vapor at different temperatures and times. The resultant nitrogen/boron codoped graphene nanoribbons (CN_x/CB_x-GNRs) are characterized and examined as electrocatalysts for ORR in an alkaline electrolyte. Our results show that the multifaceted structures of these nanoribbons can significantly enhance the ORR performance even more than longitudinal unzipped structures under the same chemical and codoping treatments. The CN_x/CB_x-GNRs with helical structures can also compete with the commercial benchmark Pt/C (20%) electrocatalyst in almost all of the key ORR properties.

RESULTS AND DISCUSSION

Longitudinal unzipping of open channel MWCNTs via chemical oxidation has been extensively studied in the past few years,[31−34] however unzipping of bamboo structures in CN_x-MWCNTs remained a challenge.[35,36] In our recent works, we have shown helical unzipping of bamboo compartments in CN_x-MWCNTs using a chemical oxidation method.[28−30] The resultant product was CN_x-GONRs with multifaceted structure. Here, we used the same unzipping protocol (Supporting Information, SI, Experiments) to generate these structures and we apply them for electrocatalyst in ORRs. Figure 1 shows schematics and high resolution electron microscopy images of the starting CN_x-MWCNTs (Figure 1a−c, left column) and the final CN_x/CB_x-GNRs with a helically unzipped structure (Figure 1a−c, right column). The average length and diameter of CN_x-MWCNTs were 50 μm and 30 nm, respectively. As observed in many HRTEM micrographs (e.g., Figure 1c, left), CN_x-MWCNTs have numerous capped short carbon nanotubes inside the main tube, referred to as "bamboo", a characteristic that differentiates them from the usual open-channel MWCNTs. Upon oxidation and unzipping, helical cleavage around the main axis could be detected, which results in a multifaceted structure along the edges of the nanoribbons (Figure 1a−c, right column). The resultant 3D GNR structures are generally few layers of graphene (Figure 1c right, light gray), although the 2D HRTEM images look thicker in some parts of the structure (Figure 1c right, dark gray). It was frequently observed throughout the HRTEM imaging process that once the entire body of the GNRs was exposed to the electron beam, beam-induced movement in the GNRs results in making some portions appear thicker (darker) than the other portions. Nitrogen functional groups, structural defects, geometrical complexity of bamboo compartments and the random distribution of chirality of each concentric graphitic shell in CN_x-MWCNTs may be responsible for such complicated unzipping. We have already proposed an unzipping mechanism based on the intercalation of species between the graphitic walls of the nanotube structure.[28−30] Intercalation of hydrosulfate anions and subsequent insertion of the oxidizing molecules increase the pressure between the carbon nanotube walls, which eventually results in helical unzipping of bamboo structures, depending on the location that hydrosulfate anions attack the short caps. The helically unzipped structures have many more edges along the length of the nanoribbon than the longitudinally unzipped open channel MWCNTs. These extra edges provide additional active sites for the oxygen reduction in the final electrocatalyst. The ideal condition would be to have GNRs completely and tightly helically opened with fully exfoliated morphologies so that all edges could contribute to the electrocatalytic reactions.

In order to study the oxygen, nitrogen, and boron surface functionalities after oxidation and codoping processes, all samples were analyzed by XPS. Figure 2 shows the XPS survey

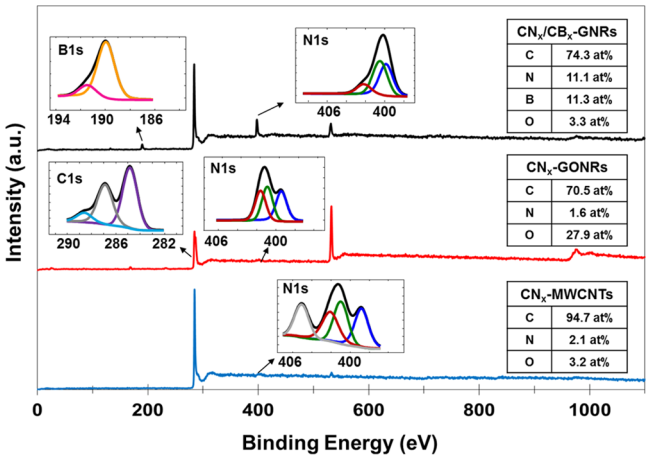

Figure 2. XPS survey of the original nitrogen doped carbon nanotubes (CN_x-MWCNTs, bottom, blue), nitrogen doped graphene oxide nanoribbons (CN_x-GONRs, middle, red) and nitrogen/boron codoped graphene nanoribbons at 900 °C for 2 h (CN_x/CB_x-GNRs, top, black). Insets are high resolution deconvoluted spectra of N 1s (pyridinic 398.8 eV, pyrrolic 401.0 eV, quaternary 402.1 eV, intercalated nitrogen molecules 405.2 eV), C 1s (C═C 284.4−284.8 ev, epoxy 286.7−287.0 eV, and carboxyl 288.8−289.1 eV) and B 1s (BC_3 189.5−190.0 ev and BC_2O 191.0−191.6 ev).

together with some of the important high resolution spectra (N 1s, C 1s, and B 1s) of the CN_x-MWCNTs, CN_x-GONRs, and CN_x/CB_x-GNRs. It is evident from the N 1s deconvoluted peaks of the CN_x-MWCNTs (Figure 2, blue spectrum on the bottom) that nitrogen incorporated into the hexagonal carbon structure in four main configurations: pyridinic (398.8 eV), pyrrolic (401.0 eV), quaternary (402.1 eV), and intercalated nitrogen molecules and/or oxides (405.2 eV). After oxidation (CN_x-GONRs), the N 1s peak associated with the intercalated nitrogen molecules and/or oxides trapped inside the nanotube structure disappears (Figure 2, red spectrum at the middle). This is an indication of successful opening of the bamboo

DOI: 10.1021/acsami.5b01067
ACS Appl. Mater. Interfaces 2015, 7, 7786−7794

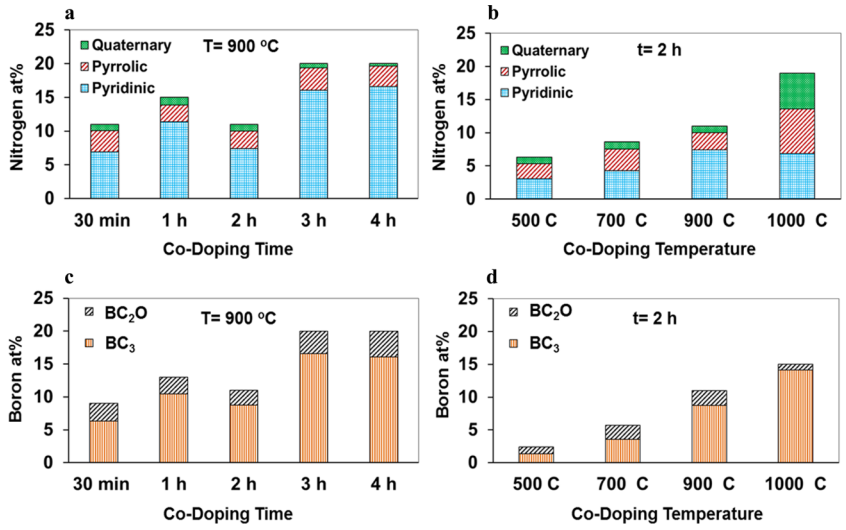

Figure 3. Effect of codoping time (30 min to 4 h) and temperature (500 to 1000 °C) on nitrogen (a,b) and boron (c,d) at% and their functional groups in CN_x/CB_x-GNRs samples.

structures, although there might still be some residual bamboo MWCNTs with diameter of about 15 nm (Figure 1c, right). It seems that the deconvoluted peak at 405.2 eV (Figure 2) is mainly due to the formation of nitrogen species in the larger diameter tubes (>20 nm), which became undetectable after cutting the nanotube structure. These observations are in close agreement with the previous report by Silva et al.[36] In addition, the deconvolution of C 1s peak of CN_x-GONRs represents that the oxygen functional species are predominantly in the form of epoxy (C—O, 286.7–287.0 eV) and carboxyl (O═C—OH, 288.8–289.1 eV) groups. Note that all spectra were calibrated with a binding energy of 284.8 eV for C═C bond. Upon exposure of CN_x-GONRs to ammonia (NH_3) gas and boron oxide (B_2O_3) vapor at 900 °C for 2 h (SI Experiments), a significant amount of nitrogen and boron species were added into the graphene nanoribbon structure (Figure 2, black spectrum on the top). In this study, boric acid powder (H_3BO_3) was used as the boron precursor. H_3BO_3 dehydrates and decomposes to water steam and metaboric acid (HBO_2) at ~170 °C. Further heating above 300 °C will result in the formation of more steam and a thermally stable compound, boron oxide (B_2O_3), which is a white glassy solid with a melting point of 450 °C and boiling point of 1860 °C. The N 1s deconvoluted peaks of the CN_x/CB_x-GNRs indicate that nitrogen is mainly contributed in the form of pyridinic and pyrrolic functional groups, and only small amount of nitrogen is quaternary. However, the B 1s peak shows that boron is mainly in the form of BC_3 groups (189.5–190.0 ev), while a slight signal for BC_2O groups (191.0–191.6 ev) could also be detected. Theoretical calculations showed that BC_3 is the most stable and uniformly distributed compound of boron–carbon 2D structure with a semiconducting behavior.[37]

To further explore the effect of codoping conditions on the concentration of nitrogen and boron, and their functionalities, a series of experiments have been conducted at different annealing times and temperatures with the results shown in Figure 3. A comparison between Figure 3, parts a and b, indicates that the effect of codoping time on nitrogen at% and species is significantly different from the effect of temperature. An increase in annealing time from 30 min to 4 h at 900 °C increases the nitrogen at% and pyridinic concentration except for a curious drop at 2 h annealing to the values equal to the sample codoped for 30 min (Figure 3a). Note that the concentration of other nitrogen functional groups (i.e., pyrrolic and quarternary) remained almost constant versus codoping time. Increasing codoping temperature from 500 to 1000 °C continuously increases the nitrogen at% (Figure 3b); the pyridinic concentration reaches a constant value at 900 °C and then the pyrrolic and quarternary proportions start increasing at higher temperature. We have previously shown a decrease of nitrogen at% in a single-doped CN_x-GNRs above 700 °C, mainly due to the formation of N_2 rather than nitrogen atoms, and also more stable C—C bonding than C—N bonding at higher temperatures.[29] However, here GNRs are exposed simultaneously to both nitrogen and boron doping sources. This facilitates the formation of boron–carbon–nitrogen (BCN) networks, in particular along the edges of graphene. This might be responsible for such high levels of nitrogen concentration at higher temperatures which is also previously reported for nitrogen/boron codoped graphene sheets.[18] The effect of codoping time and temperature on boron at% and functional groups are shown in Figure 3, parts c and d, respectively. As discussed earlier about B 1s deconvoluted spectra in Figure 2, boron functional groups in all CN_x/CB_x-GNRs samples are mainly in the form of BC_3 and BC_2O. Similar to the trend seen for nitrogen, an increase in codoping time and temperature results in a significant increase in boron at% and BC_3 groups, except for the sample codoped at 900 °C for 2 h. In the following sections, it will be shown that the CN_x/CB_x-GNRs sample codoped at 900 °C for 2 h has the best ORR performance. An optimum combination of the dopants' concentration to form a uniform BCN network and sufficient amounts of pyridinic and BC_3 functional groups are presumably the reasons for such outstanding performance. The effects of single (nitrogen or boron) and two-step doping procedures on the functionalities are also investigated and shown in SI Figure S1. Unlike codoped GNRs, only very limited amount of dopants have been incorporated into the single-doped GNRs and two-step-doped GNRs, which results in lower ORR performance.

The effects of oxidation/unzipping and nitrogen/boron codoping on the crystalline structure and defects of the starting

DOI: 10.1021/acsami.5b01067
ACS Appl. Mater. Interfaces 2015, 7, 7786–7794

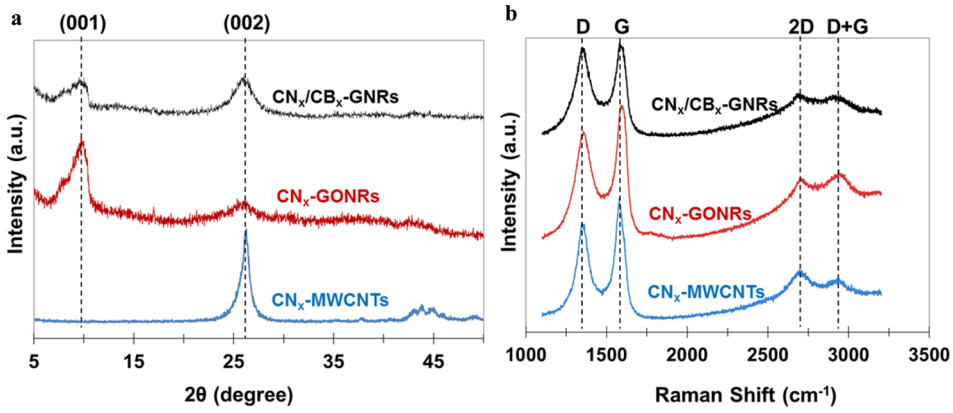

Figure 4. (a) XRD and (b) Raman spectra of the original bamboo structured nitrogen doped carbon nanotubes (CN_x-MWCNTs), nitrogen doped graphene oxide nanoribbons (CN_x-GONRs) with helically unzipped structure and nitrogen/boron codoped graphene nanoribbons at 900 °C for 2 h (CN_x/CB_x-GNRs).

CN_x-MWCNTs, CN_x-GONRs, and CN_x/CB_x-GNRs are studied using X-ray diffraction (XRD) patterns and Raman spectra, as shown in Figure 4. A very sharp graphitic (002) peak in XRD pattern of CN_x-MWCNTs is evident at 26.24° corresponding to a *d*-spacing of 3.4 Å (Figure 4a). Upon oxidative intercalation of the bamboo structures and successful helical unzipping, a very strong, but slightly broader (001) peak in CN_x-GONRs is observed at 9.78° which corresponds to a *d*-spacing of 9.1 Å. Note, the graphitic (002) peak almost disappeared. The presence of a sharp and strong (001) peak in CN_x-GONRs is an indication of a long-range, highly ordered structure subjected to a *c*-axis expansion which preserves the ordered stacking of constituent graphitic walls of the carbon nanotubes.[28,32,36] The increase in spacing from 3.4 Å in CN_x-MWCNTs to 9.1 Å in CN_x-GONRs is probably due to the insertion of oxygen atoms within the oxidized walls of carbon nanotubes in addition to the existing sulfuric acid intercalated molecules. The intensity of (001) peak, however, decreases after codoping due to the reduction and possible restacking of the intercalated layers (Figure 4a, CN_x/CB_x-GNRs). Note also that the graphitic (002) peak after codoping is still very weak and broad, representing the permanent formation of the GNRs structure. Figure 4b also indicates the Raman spectra for the same samples. A very strong D-band, comparable to G-band (I_D/I_G = 0.79, A_D/A_G = 0.82), is observed for CN_x-MWCNTs owing to the incorporation of nitrogen species into the nanotube structure. *I* and *A* represent the intensity and area of each band, respectively. After oxidation/unzipping (CN_x-GONR), the G-band is slightly blue-shifted mainly due to the incorporation of many oxygen groups and structural defects into the basal plane, and more importantly into the edges of the faceted structure. Nitrogen/boron codoping can further increase the intensity of the D-band (I_D/I_G = 0.97, A_D/A_G = 1.04) as a result of the formation of BCN network (CN_x/CB_x-GNRs). In addition, the 2D-band becomes weaker after codoping, as compared with the parent CN_x-MWCNTs. Discerning the effect of doping on the intensity of the 2D-bands in graphene (I_{2D}) is still a challenge.[38]

A comprehensive study of the ORR performance of the samples as a function of the structural features and nitrogen/boron codoping have been conducted in an alkaline electrolyte for the possible applications in alkaline fuel cells. Figure 5 shows the cyclic voltammograms (CV) of the starting CN_x-MWCNTs, CN_x-GONRs, and CN_x/CB_x-GNRs after 200

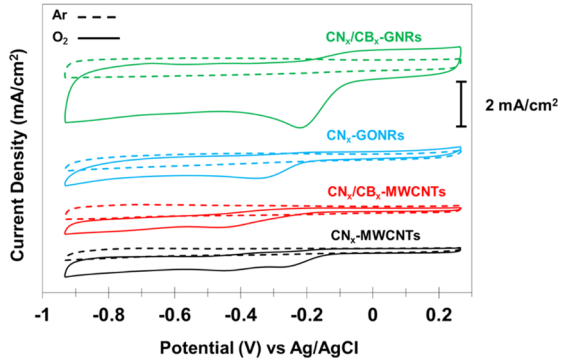

Figure 5. CV of the original nitrogen doped carbon nanotubes (CN_x-MWCNTs), nitrogen/boron codoped carbon nanotubes at 900 °C for 2 h (CN_x/CB_x-MWCNTs), nitrogen doped graphene oxide nanoribbons (CN_x-GONRs), and nitrogen/boron codoped graphene nanoribbons at 900 °C for 2 h (CN_x/CB_x-GNRs). Measurements were done in O_2-saturated (solid curves) and Ar-saturated (dashed curves) 0.1 M solution of NaOH at room temperature and a scanning rate of 100 mV/s.

cycles in O_2-saturated and Ar-saturated 0.1 M solution of NaOH at a scanning rate of 100 mV/s. For comparison, CV of the starting CN_x-MWCNTs codoped by nitrogen and boron at 900 °C for 2 h is also shown, termed CN_x/CB_x-MWCNTs. While all samples demonstrate a pure capacitive current background in Ar-saturated electrolyte (dashed curves), an obvious broad cathodic peak in O_2-saturated electrolyte associated with the oxygen reduction can be detected (solid curves). In particular, CN_x/CB_x-GNRs codoped at 900 °C for 2 h has the largest cathodic peak potential (at −0.2 V) and current density, representing an exceptional ORR catalytic performance.

The electrocatalytic properties of the selected samples together with the Pt/C (20%) sample are further explored via linear sweep voltammetry (LSV) at a disk rotation speed of 900 rpm in O_2-saturated 0.1 M solution of NaOH at a scanning rate of 5 mV/s (Figure 6a). To compare the effect of helical unzipping with longitudinal unzipping on the ORR performance, open channel undoped MWCNTs (from NTL, C-grade) were also chemically oxidized/longitudinally unzipped and nitrogen/boron codoped using the same protocol for the preparation of CN_x/CB_x-GNRs (900 °C for 2 h). The final sample is named CN_x/CB_x-Lon-GNRs in Figure 6a. The results

DOI: 10.1021/acsami.5b01067
ACS Appl. Mater. Interfaces 2015, 7, 7786−7794

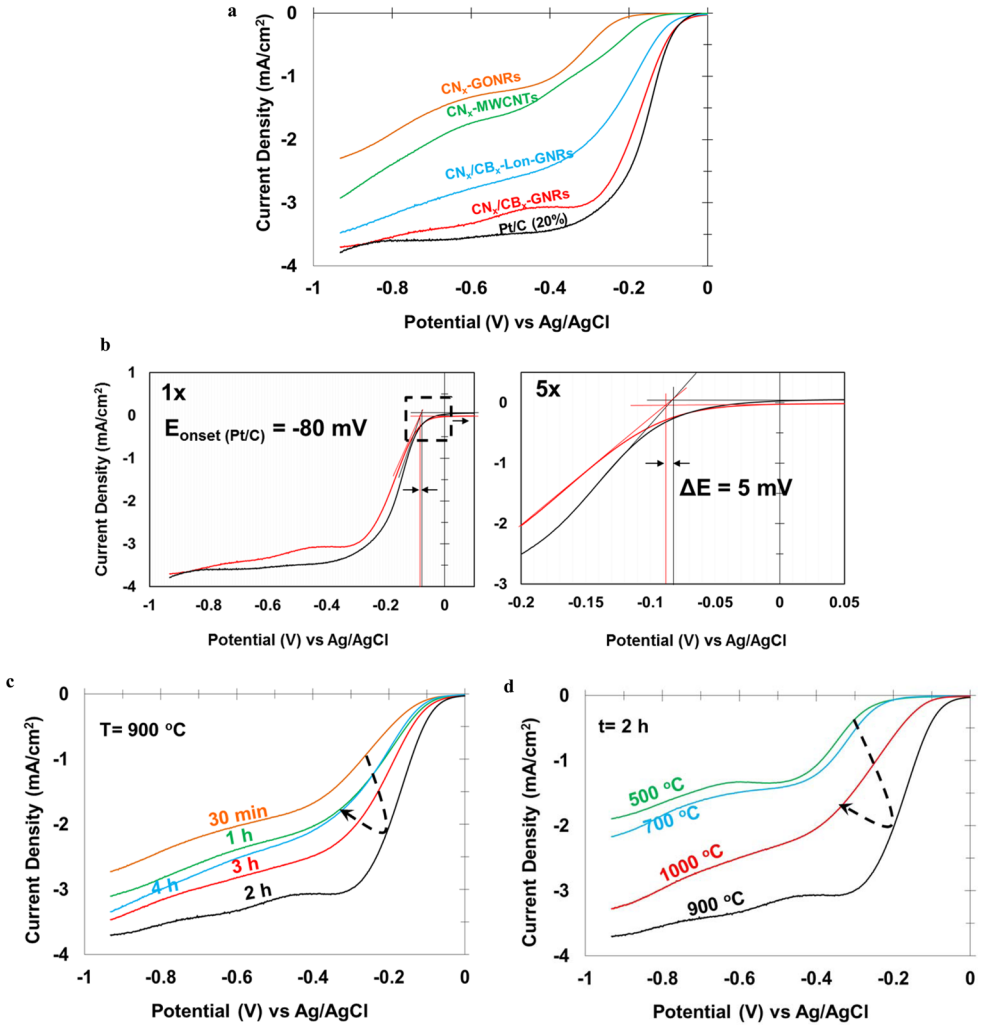

Figure 6. Linear sweep voltammetry (LSV) of (a) different carbon based electrocatalysts compared to Pt/C (20%), (b) onset potential calculations for CN_x/CB_x-GNRs (red) and Pt/C (20%) (black) at 1× and 5× magnifications of their LSV curves, (c) the effect of nitrogen/boron codoping time (30 min to 4 h) at 900 °C and (d) the effect of nitrogen/boron codoping temperature (500 to 1000 °C) for 2 h on their ORR performance. All ORR measurements were done in O_2-saturated 0.1 M solution of NaOH at electrode rotation speed of 900 rpm at room temperature and scanning rate of 5 mV/s.

show the excellent ORR performance of the CN_x/CB_x-GNRs sample compared to the parent CN_x-MWCNTs and CN_x-GONRs due to the synergistic effects of nitrogen/boron codoping and the active sites on the edges of the nanoribbons. In particular, helically unzipped sample (CN_x/CB_x-GNRs) has even larger exchange current density and lower onset potential than the longitudinally unzipped structure (CN_x/CB_x-Lon-GNRs) after similar chemical and annealing treatments. This is mainly due to the faceted structure of GNRs and the increased edges with helical unzipping, thereby providing further active sites for oxygen reduction. An onset potential of −80 mV and a current density of −3.75 mA/cm^2 for this sample are two of the key ORR properties that are almost equal to the Pt/C (20%) sample (Figure 6b). The single-doped (CN_x-GNRs, CB_x-GNRs) and two-step-doped (CN_x/CB_x-GNRs-Two Step) samples show lower ORR performance than the codoped samples (SI Figures S2 and S3). The effects of codoping time and temperature on the ORR performance are also investigated and shown in Figure 6, parts c and d, respectively. It is evident that an increase in codoping time and temperature can improve the performance up to an optimum point (2 h at 900 °C), and beyond this point, the performance and codoping are inversely related, as are performance and temperature. As it is shown in Figure 3, the nitrogen and boron concentrations for this CN_x/CB_x-GNRs sample are equal, each having 11 at%. A good ORR performance for nitrogen/boron codoped graphene was also reported previously by Wang et al.[18] at the same dopants concentrations, suggesting the formation of a uniform BCN network. According to their DFT calculations, the substitution of carbon in a graphene network by nitrogen and boron leads to a smaller energy gap, and therefore higher conductivity and ORR performance. However, overdoping by nitrogen and boron (>12 at%) results in a significant increase in the energy gap, lower electron transfer and poorer ORR performance. At lower nitrogen and boron concentrations (<8 at%), dopants distributed randomly with no possible BCN network or in small BN clusters. Note that not all nitrogen and boron functional groups can enhance the ORR performance. Several experimental and theoretical works have reported that the carbon atoms in the nearby pyridinic nitrogen groups, particularly on the edges, are much more electrochemically active than pyrrolic and quaternary nitrogen.[5,6,16] It was also found that BC_3 is the most active boron group in graphene for ORR application.[18,19]

DOI: 10.1021/acsami.5b01067
ACS Appl. Mater. Interfaces 2015, 7, 7786−7794

In order to calculate the electron transfer number and kinetic current density, the other two key ORR properties, LSV measurements were performed for some selected samples at different disk rotation speeds from 225 to 1600 rpm in O_2-saturated 0.1 M solution of NaOH. For example, Figure 7a shows the LSV curves at different rotation speeds for the CN_x/CB_x-GNRs sample codoped at 900 °C for 2 h. There is a direct relationship between the measured current density and the electrode rotation speed. The higher the rotation speed, the shorter the diffusion distance, and the larger the current density. The LSV curves at different rotation speeds for the Pt/C (20%) sample are also shown in SI Figure S4. The Koutecky–Levich plots (Figure 7b for the CN_x/CB_x-GNRs and SI Figure S5 for the Pt/C (20%)) were generated from the polarization curves at different potentials according to the following equation:

$$\frac{1}{J} = \frac{1}{J_k} + \frac{1}{B\omega^{0.5}} \quad (1)$$

where J is the measured current density (mA/cm^2), J_k is the kinetic current density (mA/cm^2), B is the reciprocal of the slope, and ω is the angular electrode rotation speed (rad/s). An excellent linearity of the plots and the nearly parallel fitted lines at each potential are indications of the first-order reaction kinetics and constant electron transfer number at different potentials.[26] The electron transfer number (n) can be calculated from the slopes of the lines using the following equation:

$$B = 0.2nF\nu^{-1/6}D_{O_2}^{2/3}C_{O_2} \quad (2)$$

where F is the Faraday constant (96485 C/mol), ν is the kinematic viscosity of the electrolyte (0.01 cm^2/s),[26] D_{O_2} is the diffusion coefficient of oxygen (2.2×10^{-5} cm^2/s) and C_{O_2} is the concentration of oxygen in the bulk (1.38×10^{-6} mol/cm^3).[39] Note that the constant 0.2 in eq 2 is adjusted as the rotation speed in eq 1 is expressed in rpm. The results of the calculations of electron transfer numbers and kinetic current densities for the Pt/C (20%), CN_x/CB_x-GNRs codoped at 900 °C (for 30 min, 1 h, 2 h) and CN_x/CB_x-Lon-GNRs codoped at 900 °C for 2 h are shown in Figure 7c. It is evident that the CN_x/CB_x-GNRs sample codoped at 900 °C for 2 h exhibits predominantly four-electron transfer for ORR (n = 3.91), very close to the Pt/C (20%) sample (n = 3.97). The CN_x/CB_x-Lon-GNRs sample (n = 2.74) and the CN_x/CB_x-GNRs samples codoped for 30 min (n = 2.31) and 1 h (n = 2.73), however, have a combined two-electron and four-electron reduction pathway, which is not efficient for the ORR applications. The kinetic current densities (J_k) for the CN_x/CB_x-GNRs and the CN_x/CB_x-Lon-GNRs samples codoped at 900 °C for 2 h are not still as high as the Pt/C (20%) sample, although they are among the highest values that have been reported for graphene-based nanomaterials.[16,19,26]

One of the key ORR properties of the electrocatalysts is their stability over time. Figure 8 represents the stability of the best CN_x/CB_x-GNRs sample (codoped at 900 °C for 2 h) compared with the Pt/C (20%) sample using a chronoampero-

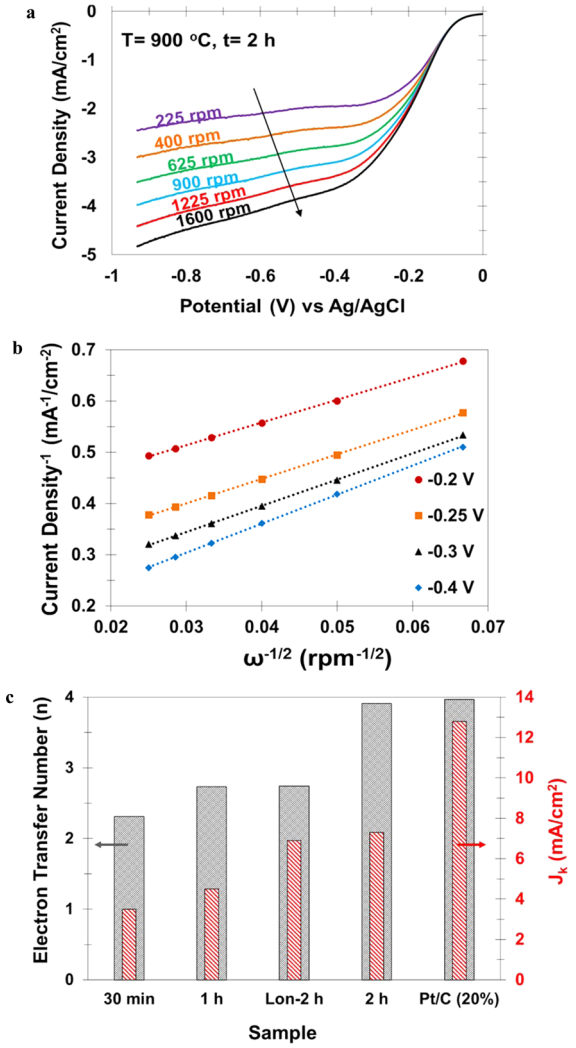

Figure 7. (a) LSV curves of nitrogen/boron codoped graphene nanoribbons at 900 °C for 2 h (CN_x/CB_x-GNRs) at different electrode rotation speeds (225 to 1600 rpm), (b) Koutecky–Levich plots of the same sample at different potentials obtained from LSV curves and (c) the electron transfer number (n, left black axis) and the kinetic limiting current density (J_k, right red axis) of CN_x/CB_x-GNRs codoped at 900 °C for 30 min, 1 and 2 h compared to Pt/C (20%). Lon-2 h stands for the CN_x/CB_x-Lon-GNRs sample codoped at 900 °C for 2 h where the original carbon nanotube was undoped and longitudinally unzipped after oxidation. LSV measurements were done in O_2-saturated 0.1 M solution of NaOH at a scanning rate of 5 mV/s.

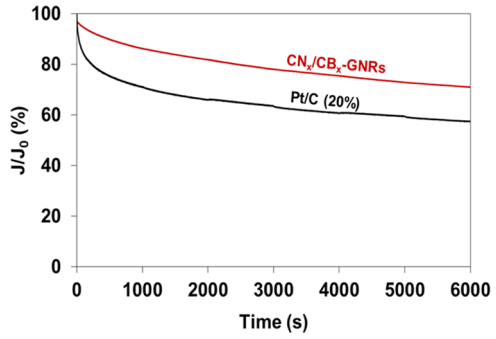

Figure 8. Chronoamperometry responses of the CN_x/CB_x-GNRs codoped at 900 °C for 2 h compared to Pt/C (20%) at constant potential −0.2 V in O_2 saturated 0.1 M solution of NaOH. Both samples were tested at the electrode rotation speed of 900 rpm at room temperature. J is the instant current density, and J_0 is the initial current density (time = 0 s).

DOI: 10.1021/acsami.5b01067
ACS Appl. Mater. Interfaces 2015, 7, 7786–7794

metric measurement technique at a constant potential of −0.2 V after 6000 s. Evidently, the nitrogen/boron codoped graphene nanoribbon developed in this research has a substantially better stability of current density than the state-of-the-art Pt/C (20%) catalyst. This great performance could indeed be attributed to the stable uniformly distributed BCN networks in the multifaceted structure of the graphene nanoribbons.

In addition to the excellent ORR performance, the CN_x/CB_x-GNRs in this work might have potential applications in metal−air batteries as a bifunctional electrocatalyst, where good oxygen evolution reaction (OER) properties are also required. Therefore, the OER performance of the CN_x/CB_x-GNRs samples together with the Pt/C (20%) sample after the first cycle are evaluated via LSV method in the potential range from 0.0 to 0.87 V (vs Ag/AgCl) in 0.1 M solution of NaOH at scanning rate of 5 mV/s. As shown in Figure 9, the OER

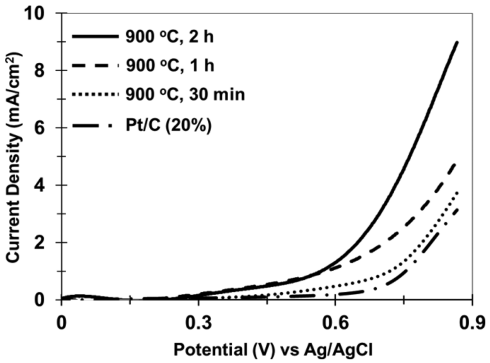

Figure 9. LSV curves of oxygen evolution of the CN_x/CB_x-GNRs codoped at 900 °C for 30 min, 1 h, and 2 h compared to Pt/C (20%) in 0.1 M solution of NaOH at scanning rate of 5 mV/s.

current density for the CN_x/CB_x-GNRs sample codoped at 900 °C for 2 h is 9 mA/cm^2 at 0.87 V (vs. Ag/AgCl), which is indeed one of the highest current densities that have ever been reported for the graphene-based OER electrocatalysts.[40−42] As one of the most important considerations for applications in metal−air batteries, however, the OER performance of the CN_x/CB_x-GNRs sample after 50 cycles is very poor (SI Figure S6). Incorporation of metal atoms into the GNR network, "metal-doping", or decoration of the GNR with some metallic nanoparticles are the main strategies that we are currently studying to improve the OER durability of the samples.

CONCLUSIONS

CN_x-MWCNTs with bamboo structures have been successfully unzipped using potassium permanganate and trifluoroacetic acid. The resultant CN_x-GONRs have a multifaceted structure due to the helical unzipping mechanism of bamboo compartments. From the N 1s XPS spectra, it can be realized that the peak associated with the nitrogen intercalated molecules and/or oxides trapped inside the nanotube disappeared after oxidation, indicating successful opening of the structure. The results showed that the CN_x/CB_x-GNRs codoped at 900 °C for 2 h can compete with the Pt/C (20%) electrocatalyst in all of the key ORR properties: onset potential, exchange current density, four electron pathway selectivity, kinetic current density and stability. This excellent ORR performance is mainly due to the synergistic effects of nitrogen/boron codoping and multifaceted structure of the graphene nanoribbons with helical unzipping mechanism. In agreement with the previous studies on graphene nanomaterials, pyridinic and BC_3 functional groups are the main active sites in the CN_x/CB_x-GNRs sample that can particularly enhance the ORR performance. The CN_x/CB_x-GNRs codoped at 900 °C for 2 h also showed an outstanding current density for oxygen evolution reaction, although the durability needs to be further improved. Due to the formation of many nanoscale p−n junctions in the structure, CN_x/CB_x-GNRs might have potential application as photocatalysts for hydrogen generation in solar cells.

ASSOCIATED CONTENT

Supporting Information

Details of the experiments, the XPS and ORR results of single and two-step doped GNRs, the ORR properties of the Pt/C (20%) sample and the OER performance of CN_x/CB_x-GNRs after 50 cycles. This material is available free of charge via the Internet at http://pubs.acs.org.

AUTHOR INFORMATION

Corresponding Authors

*E-mail: u.sundararaj@ucalgary.ca (U.S.).
*E-mail: tour@rice.edu (J.T.).

Present Address

[⊥]KU-KIST Graduate School of Converging Science & Technology. Korea University, 145, Anam-ro, Seongbuk-gu, Seoul 136-701, Republic of Korea.

Notes

The authors declare no competing financial interest.

ACKNOWLEDGMENTS

This research is financially supported by the Natural Sciences and Engineering Research Council of Canada (NSERC) and Alberta Innovates Technology Futures (AITF). This work is also financially supported by Air Force Office of Scientific Research (AFOSR), FA9550-14-1-0111.

REFERENCES

(1) Zhang, J. *PEM Fuel Cell Electrocatalysts and Catalyst Layers: Fundamentals and Applications*; Springer-Verlag London Ltd: London, UK, 2008; Chapter 2, pp 89−135.
(2) Chabot, V.; Higgins, D.; Yu, A.; Xiao, X.; Chen, Z.; Zhang, J. A Review of Graphene and Graphene Oxide Sponge: Materials Synthesis and Applications to Energy and the Environment. *Energy Environ. Sci.* **2014**, *7*, 1564−1596.
(3) Zhu, J.; Yang, D.; Yin, Z.; Yan, Q.; Zhang, H. Graphene and Graphene-Based Materials for Energy Storage Applications. *Small* **2014**, *10*, 3480−3498.
(4) Yu, D.; Nagelli, E.; Du, F.; Dai, L. Metal-Free Carbon Nanomaterials Become More Active that Metal Catalysts and Last Longer. *J. Phys. Chem. Lett.* **2010**, *1*, 2166−2173.
(5) Jiao, Y.; Zheng, Y.; Jaroniec, M.; Qiao, S. Z. Origin of the Electrocatalytic Oxygen Reduction Activity of Graphene-Based Catalysts: A Roadmap to Achieve the Best Performance. *J. Am. Chem. Soc.* **2014**, *136*, 4394−4403.
(6) Wang, H.; Maiyalagan, T.; Wang, X. Review on Recent Progress in Nitrogen-Doped Graphene: Synthesis, Characterization, and Its Potential Applications. *ACS Catal.* **2012**, *2*, 781−794.
(7) Brownson, D.; Kampouris, D. K.; Banks, C. E. Graphene Electrochemistry: Fundamental Concepts Through to Prominent Applications. *Chem. Soc. Rev.* **2012**, *41*, 6944−6976.
(8) Daems, N.; Sheng, X.; Vankelecom, I. F. J.; Pescarmona, P. P. Metal-Free Doped Carbon Materials as Electrocatalysts for the Oxygen Reduction Reaction. *J. Mater. Chem. A* **2014**, *2*, 4085−4110.

DOI: 10.1021/acsami.5b01067
ACS Appl. Mater. Interfaces 2015, 7, 7786−7794

(9) Tang, L.; Wang, Y.; Li, Y.; Feng, H.; Lu, J.; Li, J. Preparation, Structure, and Electrochemical Properties of Reduced Graphene Sheet Films. *Adv. Funct. Mater.* **2009**, *19*, 2782−2789.
(10) Shao, Y.; Zhang, S.; Engelhard, M. K.; Li, G.; Shao, G.; Wang, Y.; Liu, J.; Aksay, I. A.; Lin, Y. Nitrogen-Doped Graphene and Its Electrochemical Applications. *J. Mater. Chem.* **2010**, *20*, 7491−7496.
(11) Qu, L.; Liu, Y.; Baek, J. B.; Dai, L. Nitrogen-Doped Graphene as Efficient Metal-Free Electrocatalyst for Oxygen Reduction in Fuel Cells. *ACS Nano* **2010**, *4*, 1321−1326.
(12) Sheng, Z. H.; Shao, L.; Chen, J. J.; Bao, W. J.; Wang, F. B.; Xia, X. H. Catalyst-Free Synthesis of Nitrogen-Doped Graphene via Thermal Annealing Graphite Oxide with Melamine and Its Excellent Electrocatalysis. *ACS Nano* **2011**, *5*, 4350−4358.
(13) Geng, D.; Chen, Y.; Chen, Y.; Li, Y.; Li, R.; Sun, X.; Ye, S.; Knights, S. High Oxygen-Reduction Activity and Durability of Nitrogen-Doped Graphene. *Energy Environ. Sci.* **2011**, *4*, 760−764.
(14) Luo, Z.; Lim, S.; Tian, Z.; Shang, J.; Lai, L.; MacDonald, B.; Fu, C.; Shen, Z.; Yu, T.; Lin, J. Pyridinic N Doped Graphene: Synthesis, Electronic Structure, and Electrocatalytic Property. *J. Mater. Chem.* **2011**, *21*, 8038−8044.
(15) Lin, Z.; Waller, G. H.; Liu, Y.; Liu, M.; Wong, C. P. Simple Preparation of Nanoporous Few-Layer Nitrogen-Doped Graphene for Use as an Efficient Electrocatalyst for Oxygen Reduction and Oxygen Evolution Reactions. *Carbon* **2013**, *53*, 130−136.
(16) Xing, T.; Zheng, Y.; Li, L. H.; Cowie, B. C. C.; Gunzelmann, D.; Qiao, S. Z.; Huang, S.; Chen, Y. Observation of Active Sites for Oxygen Reduction Reaction on Nitrogen-Doped Multilayer Graphene. *ACS Nano* **2014**, *8*, 6856−6862.
(17) Sheng, Z. H.; Gao, H. L.; Bao, W. J.; Wang, F. B.; Xia, X. H. Synthesis of Boron Doped Graphene for Oxygen Reduction Reaction in Fuel Cells. *J. Mater. Chem.* **2012**, *22*, 390−395.
(18) Wang, S.; Zhang, L.; Xia, Z.; Roy, A.; Chang, D. W.; Baek, J. B.; Dai, L. BCN Graphene as Efficient Metal-Free Electrocatalyst for the Oxygen Reduction Reaction. *Angew. Chem.* **2012**, *124*, 4285−4288.
(19) Zheng, Y.; Jiao, Y.; Ge, L.; Jaroniec, M.; Qiao, S. Z. Two-Step Boron and Nitrogen Doping in Graphene for Enhanced Synergistic Catalysis. *Angew. Chem.* **2013**, *125*, 3192−3198.
(20) Yang, S.; Zhi, L.; Tang, K.; Feng, X.; Maier, J.; Mullen, K. Efficient Synthesis of Heteroatom (N or S)-Doped Graphene Based on Ultrathin Graphene Oxide-Porous Silica Sheets for Oxygen Reduction Reactions. *Adv. Funct. Mater.* **2012**, *22*, 3634−3640.
(21) Liang, J.; Jiao, Y.; Jaroniec, M.; Qiao, S. Z. Sulfur and Nitrogen Dual-Doped Mesoporous Graphene Electrocatalyst for Oxygen Reduction with Synergistically Enhanced Performance. *Angew. Chem., Int. Ed.* **2012**, *51*, 11496−11500.
(22) Li, R.; Wei, Z.; Gou, X.; Xu, W. Phosphorus-Doped Graphene Nanosheets as Efficient Metal-Free Oxygen Reduction Electrocatalysts. *RSC Adv.* **2013**, *3*, 9978−9984.
(23) Kim, H.; Lee, K.; Woo, S. I.; Jung, Y. On the Mechanism of Enhanced Oxygen Reduction Reaction in Nitrogen-Doped Graphene Nanoribbons. *Phys. Chem. Chem. Phys.* **2011**, *13*, 17505−17510.
(24) Li, Y.; Zhou, W.; Wang, H.; Xie, L.; Liang, Y.; Wei, F.; Idrobo, J. C.; Pennycook, S. J.; Dai, H. An Oxygen Reduction Electrocatalyst Based on Carbon nanotube−Graphene Complexes. *Nat. Nanotechnol.* **2012**, *7*, 394−400.
(25) Davis, D. J.; Raji, A. R. O.; Lambert, T. N.; Vigil, J. A.; Li, L.; Nan, K.; Tour, J. M. Silver-Graphene Nanoribbon Composite Catalyst for the Oxygen Reduction in Alkaline Electrolyte. *Electroanalysis* **2014**, *26*, 164−170.
(26) Liu, M.; Song, Y.; He, S.; Tjiu, W. W.; Pan, J.; Xia, Y. Y.; Liu, T. Nitrogen-Doped Graphene Nanoribbons as Efficient Metal-Free Electrocatalysts for Oxygen Reduction. *ACS Appl. Mater. Interfaces* **2014**, *6*, 4214−4222.
(27) Chen, L.; Du, R.; Zhu, J.; Mao, Y.; Xue, C.; Zhang, N.; Hou, Y.; Zhang, J.; Yi, T. Three-Dimensional Nitrogen-Doped Graphene Nanoribbons Aerogel as a Highly Efficient Catalyst for the Oxygen Reduction Reaction. *Small* **2014**, in press, DOI: 10.1002/smll.201402472.
(28) Khajepour, M.; Sadeghi, S.; Zehtab Yazdi, A.; Sundararaj, U. Tuning the Curing Behavior of Fluoroelastomer (FKM) by Incorporation of Nitrogen Doped Graphene Nanoribbons (CNx-GNRs). *Polymer* **2014**, *55*, 6293−6302.
(29) Zehtab Yazdi, A.; Chizari, K.; Sundararaj, U. Simultaneous Thermal Reduction and Nitrogen Doping of Chemically Oxidized Graphene Nanoribbons. *248th ACS National Meeting and Exposition*, San Francisco, CA, 2014.
(30) Zehtab Yazdi, A.; Chizari, K.; Sundararaj, U. Chemical Unzipping Process of Nitrogen-Doped Carbon Nanotubes. *29th International Conference of the Polymer Processing Society (PPS)*, Nuremberg, Germany, July 16−19, 2013.
(31) Kosynkin, D. V.; Higginbotham, A. L.; Sinitskii, A.; Lomeda1, J. R.; Dimiev, A.; Price, B. K.; Tour, J. M. Longitudinal Unzipping of Carbon Nanotubes to Form Graphene Nanoribbons. *Nature* **2009**, *458*, 872−876.
(32) Higginbotham, A. L.; Kosynkin, D. V.; Sinitskii, A.; Sun, Z.; Tour, J. M. Lower-Defect Graphene Oxide Nanoribbons from Multiwalled Carbon Nanotubes. *ACS Nano* **2010**, *4*, 2059−2069.
(33) James, D. K.; Tour, J. M. Graphene: Powder, Flakes, Ribbons, and Sheets. *Acc. Chem. Res.* **2013**, *46*, 2307−2318.
(34) James, D. K.; Tour, J. M. The Chemical Synthesis of Graphene Nanoribbons—A Tutorial Review. *Macromol. Chem. Phys.* **2012**, *213*, 1033−1050.
(35) Wei, J.; Lv, R.; Guo, N.; Wang, H.; Bai, X.; Mathkar, A.; Kang, F.; Zhu, H.; Wang, K.; Wu, D.; Vajtai, R.; Ajayan, P. M. Preparation of Highly Oxidized Nitrogen-Doped Carbon Nanotubes. *Nanotechnology* **2012**, *23*, 155601.
(36) Silva, R. C.; Gomez, A. M.; Diaz, S. F.; Lopez, F. T.; Elias, A. L.; Lopez, N. P.; Muramatsu, H.; Hayashi, T.; Fujisawa, K.; Kim, Y. A.; Endo, M.; Terrones, M. Formation of Nitrogen-Doped Graphene Nanoribbons via Chemical Unzipping. *ACS Nano* **2013**, *7*, 2192−2204.
(37) Luo, X.; Yang, J.; Liu, H.; Wu, X.; Wang, Y.; Ma, Y.; Wei, S. H.; Gong, X.; Xiang, H. Predicting Two-Dimensional Boron−Carbon Compounds by the Global Optimization Method. *J. Am. Chem. Soc.* **2011**, *133*, 16285−16290.
(38) Chizari, K.; Sundararaj, U. The Effects of Catalyst on the Morphology and Physicochemical Properties of Nitrogen-Doped Carbon Nanotubes. *Mater. Lett.* **2014**, *116*, 289−292.
(39) Zagal, J.; Bindra, P.; Yeager, E. A Mechanistic Study of O_2 Reduction on Water Solubel Phthalocyanines Adsorbed on Graphite Electrodes. *J. Electrochem. Soc.* **1980**, *127*, 1506−1517.
(40) Park, H. W.; Lee, D. U.; Liu, Y.; Wu, J.; Nazar, L. F.; Chen, Z. Bi-Functional N-Doped CNT/Graphene Composite as Highly Active and Durable Electrocatalyst for Metal Air Battery Applications. *J. Electrochem. Soc.* **2013**, *160*, 2244−2250.
(41) Liang, Y.; Li, Y.; Wang, H.; Zhou, J.; Wang, J.; Regier, T.; Dai, H. Co_3O_4 Nanocrystals on Graphene as a Synergistic Catalyst for Oxygen Reduction Reaction. *Nat. Mater.* **2011**, *10*, 780−786.
(42) Jahan, M.; Liu, Z.; Loh, K. P. A Graphene Oxide and Copper-Centered Metal Organic Framework Composite as a Tri-Functional Catalyst for HER, OER, and ORR. *Adv. Funct. Mater.* **2013**, *23*, 5363−5372.

DOI: 10.1021/acsami.5b01067
ACS Appl. Mater. Interfaces 2015, 7, 7786−7794